https://doi.org/10.1016/j.apcatb.2020.119260

Self-cleaning and de-pollution efficacies of photocatalytic architectural membranes

Xiaochen Tang[1], Olivier Rosseler[2], Sharon Chen[1], Sébastien Houzé de l'Aulnoit[1], Michael J. Lussier[3], Jiachen Zhang[4], George Ban Weiss[4], Haley Gilbert[1], Ronnen Levinson[1], Hugo Destaillats[1,*]

[1] *Heat Island Group, Lawrence Berkeley National Laboratory, Berkeley, California 94720, USA*

[2] *Saint Gobain Research North America, Northboro, Massachusetts 01532, USA*

[3] *Saint Gobain Performance Plastics, Merrimack, New Hampshire 03054, USA*

[4] *Dept. of Civil and Environmental Engineering, University of Southern California, Los Angeles, California 90089, USA*

[*]Corresponding author E-mail: HDestaillats@lbl.gov

Keywords: photocatalytic membranes, cool wall, ISO Standard 22197-1, de-NO_x, soot, aging

Abstract

Photocatalytic self-cleaning “cool” roofs and walls can maintain high albedos, saving building cooling energy, reducing peak power demand, and mitigating the urban heat island effect. Other environmental benefits result from their de-polluting properties. Specimens from two different photocatalytic architectural membranes and a non-photocatalytic control were exposed alongside vertically, facing west, for two years in three California sites, and retrieved quarterly for testing. Photocatalytic materials showed excellent self-cleaning performance, retaining albedos of 0.74 – 0.75. By contrast, the control material exhibited an albedo loss of up to 0.10 units, with appreciable soiling observed by scanning electron microscopy. De-pollution capacity was assessed by quantifying NO removal and NO_x deposition rates at 60 °C. Efficacy varied with exposure location, weather conditions, and the nature of the photocatalytic material. Seasonal effects were observed, with partial inhibition during the dry season and reactivation during the rainy season.

1 Introduction

Highly reflective "cool" roofs and walls can save HVAC energy, reduce afternoon peak power demand, and improve thermal comfort [1-8]. Environmental benefits include the mitigation of the urban heat island effect by reducing outdoor air temperatures and smog formation [9-12], and slowing global warming [13]. Another benefit of cool building envelope surfaces is improving material durability by reducing damage induced by surface-temperature cycles [14]. However, those benefits can be significantly diminished over time as the albedo (solar reflectance) of building envelopes is reduced due to soiling deposition and biological growth [15-18]. For example, an evaluation of 586 roofing materials exposed in Miami (Florida) over a 3-year period showed that the mean albedo of aged products that had an initial albedo of 0.80 or higher, decreased to around 0.60 losing approximately 25% of the initial value. In the most extreme cases, aged albedo could be as low as 0.25, corresponding to a loss of up to 70% of the initial value [19].

Photocatalytic self-cleaning materials make building envelopes cooler by maintaining their initially high albedo values over long periods of times. Several photocatalytic products are used in construction, including cementitious coatings (such as mortar, plaster and stucco) [20-22], limestone surface treatments [23], coated metal composite siding [24], architectural membranes [25], and different roofing materials (e.g., tiles, shingles and precast panels) [26]. These represent a growing sector of the construction market. The global sales of photocatalytic products increased from US$740M in 2009 to US$1.5 billion in 2014, and are predicted to reach approximately US$2.9 billion by 2020 [27]. For these reasons, a closer examination of photocatalytic building envelope materials is warranted, to identify and quantifying benefits and limitations.

The self-cleaning effect is due to the ultraviolet (UV) light catalyzed oxidation of deposited soiling, in combination with its physical removal due to enhanced surface hydrophilicity activated by sunlight [28, 29]. Self-cleaning activity has been documented primarily in laboratory tests—e.g., by measuring the loss of deposited soot [30, 31] or bleaching of a dye applied on the surface [32, 33] as a function of UV irradiation. Tracking the dye bleaching rate is

the basis for standardized methods that quantify the self-cleaning effect [34, 35]. Superhydrophilicity (very low water contact angle) has been observed in TiO_2-coated materials under UV irradiation [36-38]. This property is used in ISO Standard 27448 to test the self-cleaning performance of photocatalytic materials [39].

An environmental benefit that has been well documented in laboratory tests is the photocatalytic elimination of atmospheric pollutants in contact with the catalyst surface, including volatile organic compounds (VOCs) [40-42] and atmospheric nitrogen oxides (NO_x = NO + NO_2) [43]. In the case of NO_x, photocatalytic oxidation enables a net removal of these species from the atmosphere through their irreversible conversion to the non-volatile oxidation byproducts nitrate (NO_3^-) and HNO_3. The final stable oxidation byproducts can be washed off the surface by rain or dew. Different test methods have been developed to evaluate the air purification efficiency of photocatalytic materials by following NO_x elimination [44-46]. One of the most commonly used is the ISO Standard 22197-1, which relies on quantifying nitric oxide (NO) elimination under controlled air flow, temperature, humidity and illumination conditions [47].

Both self-cleaning and de-polluting properties of photocatalytic construction materials have been evaluated in a number of field demonstrations. The effective removal of NO_x from urban air was demonstrated using a cement-based photocatalytic coating [22], a mineral-based paint [48], and paving materials [49, 50]. However, other studies found a significantly weaker effect [51, 52]. Photocatalytic performance can be affected by soiling deposition and loss of photocatalyst due to abrasion and material weathering [53, 54]. Some studies report a relatively low depletion of the photocatalyst, with at least 80% retention after a prolonged exposure to the environment of up to two years [55, 56]. By contrast, materials in which the photocatalyst was deposited as a coating without a strong attachment to the substrate yielded higher catalyst depletion rates [54, 57].

This study investigated the performance of photocatalytic architectural membranes exposed under real-world conditions. Architectural membranes are highly versatile materials used in building envelopes as energy-efficient roofs, façades, canopies and skylights that provide

diffuse natural daylight to indoor environments. In addition to reducing their albedo, soiling deposition onto translucent membranes can reduce the fraction of light transmitted through the material [58, 59]. For that reason, photocatalytic TiO_2 coatings are promising, as they have been shown to impart self-cleaning functionalities to fabrics [60]. Membranes based on fluoropolymer materials, such as those reported here, have been shown to serve as substrates for photoactive additives that imparted self-cleaning and anti-microbial activity [61-63]. The main goal of this study was to quantify the performance of photocatalytic membrane specimens that had been aged alongside a non-photocatalytic control material. Self-cleaning properties were quantified in terms of albedo loss, and de-polluting properties were evaluated by following NO removal rate and the NO_x deposition rate as a function of exposure time. Specimens were exposed to the environment at three locations in California: Berkeley, downtown Los Angeles, and Fresno over a two-year period.

2 Methodology

2.1 Exposed materials

The architectural membrane samples used in this study, manufactured under the Sheerfill® brand name, were provided by Saint Gobain. Non-photocatalytic versions of this product, made of polytetrafluoroethylene (PTFE)-coated fiberglass, have been in use for over 45 years as roofing and façade membranes. TiO_2-coated photocatalytic membranes have been in the market for about 10 years. The two different photocatalytic materials tested here were labeled "P1" and "P2", and corresponded to standard and alternative formulations of the Sheerfill II EverClean product. General characteristics of these materials have been previously described elsewhere [64]. Specimens of each of these samples were exposed alongside a matching control sample "C1" (standard, non-catalytic Sheerfill II membrane). The C1 sample had the same characteristics as P1 and P2, except for the photocatalytic functionality. Replicate 10 cm by 10 cm specimens of each sample were prepared for exposure to the environment. These samples were a subset of a larger "Cool Walls" study, which is reported elsewhere [7]. The

corresponding codes for the Cool Walls study were CW25 (sample P1), CW26 (sample P2) and CW24 (sample C1, control). The as-received color of all samples was tan, which bleached to off-white after several weeks of solar exposure. Per manufacturer's instructions, the initial albedo of previously unexposed architectural membranes was measured on specimens that had been pre-bleached in the laboratory by exposure to UV light in a laboratory weathering apparatus (Model Q-UV, Q-Lab Corporation, Westlake, OH) for seven days. The pre-bleaching was necessary to obtain samples representative of field installations. It simulates a process which occurs under natural sunlight to turn the products from tan to white, as per the manufacturer's documentation.

2.2 Setup of exposure sites

Photocatalytic and control specimens were exposed at three sites in California:

a) BK: a roof at the Lawrence Berkeley National Laboratory in Berkeley (San Francisco Bay Area, 37.87° N, 122.27° W);

b) LA: a parking lot at the University of Southern California, in downtown Los Angeles (34.05° N, 118.24° W); and

c) FR: a ground-level, uncovered concrete surface within a site belonging to an industry partner in Fresno (Central Valley, 36.74° N, 119.79° W).

The Berkeley (BK) site was the cleanest, being far from highways and heavy traffic. On most days, the exposure site received clean air directly from the Pacific Ocean. The Los Angeles (LA) site was representative of pollution found at a large urban area. The Fresno (FR) site provided exposure to air pollutants associated with agricultural activity, typical of the Central Valley.

Exposure racks were designed and built to hold a maximum of 280 specimens, arranged in 14 rows of 20 specimens each. The rows were horizontally staggered to prevent contamination between vertically adjacent specimens. Racks were built in-situ at the three California sites between March and April 2016, and specimens from different materials were installed

immediately after their construction, including those corresponding to the architectural membrane samples P1, P2 and C1 [65]. Ten specimens of each sample were installed at each of the three sites at the onset of the experiment. Specimens were mounted vertically, facing west. Figure 1 illustrates the racks used to expose specimens, and a photo of an individual architectural membrane specimen. Given the flexibility of this material, it was kept secured against the wood backing by clamping on the top and bottom sections.

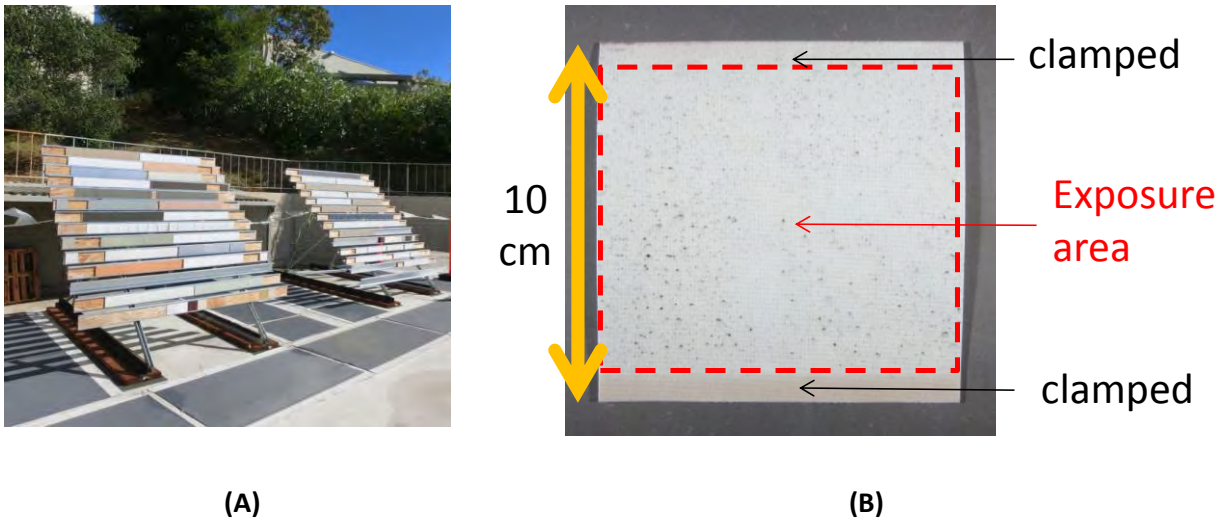

Figure 1. Images of (A) two of the three exposure racks used at the Berkeley site and (B) an architectural fabric specimen. Specimens were secured against the wood backing by clamps on the top and bottom sections.

Monthly rainfall and temperature data at each exposure site were obtained from nearby Global Historical Climatology Network (GHCN) weather stations. The data sets were downloaded from the National Oceanic and Atmospheric Administration [66]. The weather stations selected for each site were:

a) USC00040693, in Berkeley, 3.2 km southeast of the Berkeley exposure site;

142 b) USW00093134, on the University of Southern California (USC) campus, 1.4 km west of
143 the Los Angeles exposure site; and

144 c) USW00093193, at the Fresno Yosemite International Airport, 9.9 km north of the Fresno
145 exposure site

146 Similarly, monthly air pollution data for Berkeley was obtained from the California Air
147 Resources Board [67], for Los Angeles from the South Coast Air Quality Management District
148 [68], and for Fresno from the US Environmental Protection Agency [69]. Each source was
149 selected based on their closer proximity to the corresponding site.

150

151 **2.3 Experimental procedures**

152 **2.3.1 Specimen retrieval, shipping, characterization, and storage**

153 Ten identical specimens from each of the products (P1, P2 and C1) were exposed side-by-side.
154 One specimen from each sample was retrieved quarterly from each site at approximately the
155 same time, following the schedule presented in Table S1 (Supporting Information). Specimens
156 were packed in individual glassine envelopes, and shipped to LBNL for laboratory analysis. The
157 samples were stored inside the same envelopes prior and after laboratory measurements.
158 There was no exposure to the environment after the specimens were retrieved from the racks.

159 Albedo was measured on all specimens with a solar spectrum reflectometer (Version 6, Devices
160 & Services, Dallas TX), using an air mass 1.5 global vertical (sun-facing) output added by the
161 manufacturer [70]. Measurement results were reported as the average ± standard deviation of
162 multiple measurements. For the initial (unexposed) specimens, the reported standard deviation
163 corresponded to the standard deviation of three measurements performed at non-overlapping
164 locations on each specimen.

165 The image of each specimen was obtained with a digital camera (Canon PowerShot S90,
166 Melville, NY) using a setup that provided consistent lighting conditions. An 18% grey card was
167 used as the background.

168 The static water contact angle was measured on the surface of unexposed samples, and on
169 specimens that were exposed for two years on each site, with a Theta optical tensiometer
170 (Biolin Scientific, Gothenburg, Sweden) using the sessile drop method.

171 A Phenom XL scanning electron microscope (SEM, Thermo Fisher Scientific, Waltham MA) was
172 used to image the surface of samples after exposure and characterize the soiling deposition.
173 The microscope used a Back Scattered Detector (BSD) and an Energy Dispersive X-Ray
174 Spectroscopy (EDS) detector, with an acceleration voltage of 15 kV in both modes. Examination
175 of unexposed and exposed specimens allowed to evaluate the type of soiling matter deposited
176 on the samples during the exposure. In addition, SEM-EDS measurements were used to
177 evaluate the potential loss of Ti upon exposure to the environment, by comparing the Ti mass
178 fraction measured in unexposed and two-year exposed specimens.

179 **2.3.2 Measurement of the de-pollution performance**

180 The methodology used to evaluate the de-pollution performance was adapted from the
181 previously mentioned ISO Standard 22197-1 [47]. A flow of 3 L/min of laboratory air was pre-
182 treated with an activated carbon bed and a HEPA filter, and enriched with 1000 ppb nitric oxide
183 (NO) prior to entering the exposure chamber. The relative humidity (RH) was adjusted to 50%
184 by splitting the air flow, then circulating one of the flows through a water bubbler. Two mass
185 flow controllers were used to adjust the desired RH. In the exposure chamber, a specimen from
186 either sample P1, P2 or C1 was installed facing upwards in the center. A UV-A lamp with
187 maximum intensity at about 360 nm (Model TL-D, Actinic BL, Philips, Andover, MA) was used to
188 irradiate the specimen through a quartz window on the chamber's cover. The exposed surface
189 area for each specimen was 0.01 m^2. The distance between the window and the specimen was
190 5 mm. UV irradiance (320 - 400 nm; peak sensitivity at 360 nm) was measured using a digital
191 radiometer (Model UVX, UVP LLC, Upland, CA). It was highest at the center of the sample and
192 consistent over the exposed surface, with an average of 11.5 ± 1.5 W/m^2. The stability of the
193 lamp during the experimental period was verified by repeating irradiance measurements at
194 different times.

In previous work using the same setup, it was observed that raising the surface temperature from 25 °C to 60 °C increased the NO_x-removal efficacy of photocatalytic surfaces [26]. Here, the surface temperature was kept at 60 °C using an external circulating bath, to simulate conditions that are close to those found on building surfaces under the sun. Air exiting the chamber was split into two flows; one of them was directed to a chemiluminescence NO_x analyzer (Model 200A, Teledyne Technologies, Thousand Oaks, CA), which was calibrated at different times during the testing period. The other chamber air stream was used to measure air temperature and RH at the outlet prior to venting in a fume hood, using an in-line digital HIH6100 series T/RH sensor (Honeywell, Charlotte NC). NO and NO_2 concentrations at the reactor outlet, air temperature and RH in the chamber, and chamber (surface) temperature were measured at 0.2 Hz.

Tests carried out with each specimen comprised the following three segments:

a) pre-equilibration under a constant flow of NO-enriched air in the dark (about 1 h);

b) continuous UV irradiation under a constant flow of NO-enriched air (about 6 h), and

c) post-equilibration under a constant flow of NO-enriched air in the dark (about 1 h)

Figure S1 (Supporting Information) illustrates curves corresponding to typical NO and NO_2 traces. Removal rate of NO (r_{NO}, µmol h^{-1}) and formation rate of NO_2 (r_{NO_2}, µmol/h, from oxidation of NO) were calculated using the difference between the inlet and outlet concentrations of NO and NO_2, as follows:

$$r_{\mathrm{NO}} = \frac{\int_0^\tau n_{\mathrm{NO_{removed}}} dt}{\tau} = \frac{\int_0^\tau (c_{\mathrm{NO_i}} - c_{\mathrm{NO_{out}}}) dt}{\tau} \times \frac{Q}{V_n} \quad (1)$$

$$r_{\mathrm{NO_2}} = \frac{\int_0^\tau n_{\mathrm{NO_{2formed}}} dt}{\tau} = \frac{\int_0^\tau (c_{\mathrm{NO_{2out}}} - c_{\mathrm{NO_{2i}}}) dt}{\tau} \times \frac{Q}{V_n} \quad (2)$$

where Q is the flow rate (L min^{-1}), τ is the irradiation duration (h), t is the time (h) and V_n is the normalized gas volume for one mole of gas at standard pressure and room temperature (22.4 L). The NO_x deposition rate was computed as the difference between NO removal and NO_2 formation rates per unit area, expressed in moles (R_{NO_x}, μmol h^{-1} m^{-2}). Assuming that nitrate and NO_2 are the only NO oxidation byproducts, R_{NO_x} can be used to calculate the rate of nitrate formation. This prediction corresponds to the maximum nitrate formation rate that can be observed, and allows for an estimation of the maximum nitrate surface concentration, as illustrated in Figure S1-B.

3 Results and discussion

3.1 Weather and air pollution measurements at each site

Rain seasonal patterns at the three sites were similar, and are presented in Figure 2. Across the three sites we observed a dry season from April to October, followed by rainy season through the late fall, winter and beginning of spring. Additional descriptions of weather patterns at the sites are included in the Supporting Information. We also provide air pollution results in Figure S2.

232

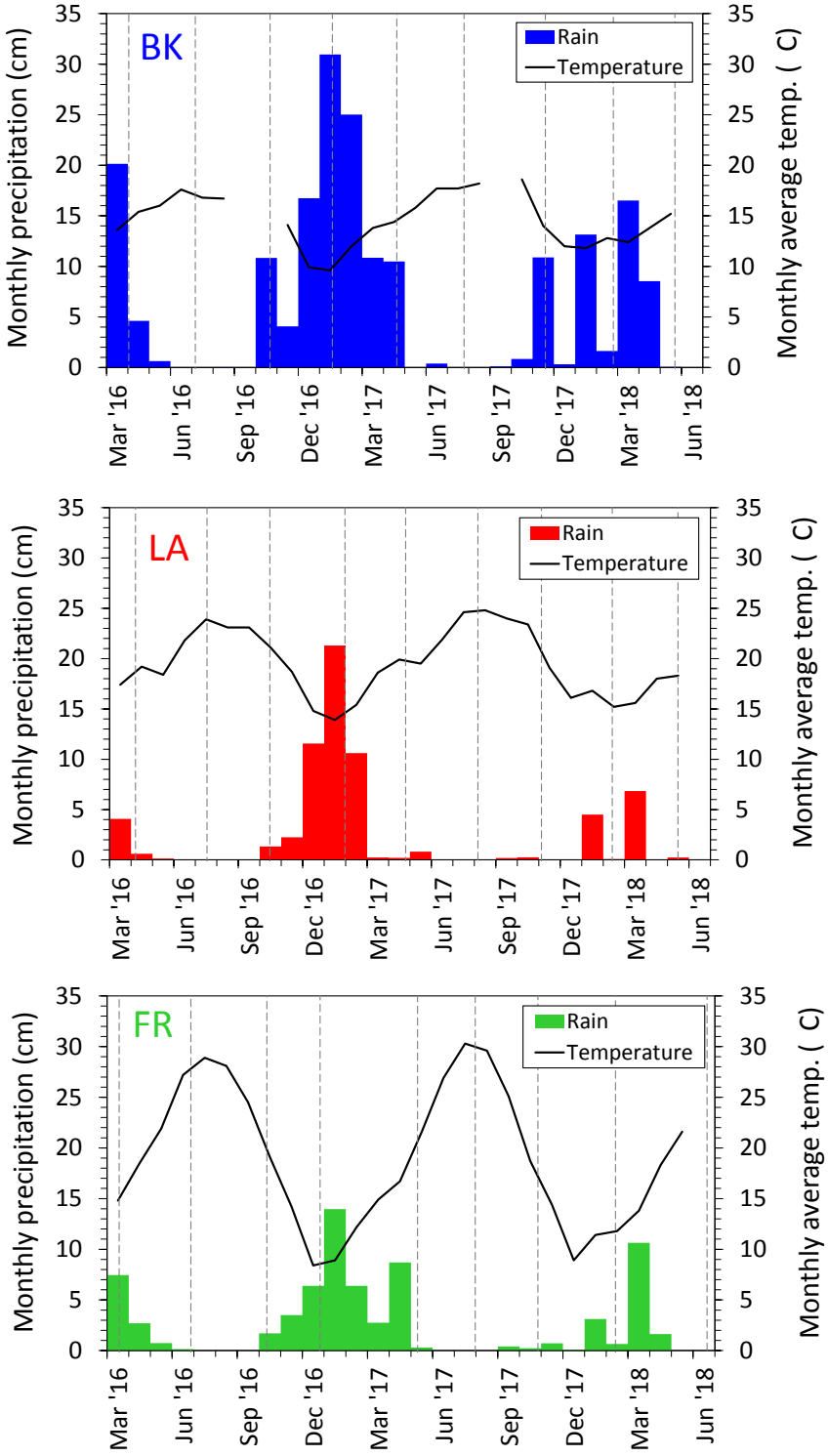

233

234 **Figure 2.** Precipitation and temperature recorded at the Berkeley (BK), Los Angeles (LA), and Fresno
235 (FR) sites. The vertical dotted lines correspond to the times at which specimens were retrieved.

3.2 Physical chemical characterization of exposed materials

3.2.1 Contact angle measurements

The water contact angle was measured on unexposed samples and on specimens retrieved after two years of exposure. Figure 3 shows results for initial (pre-bleached) specimens, and for those exposed for two years at each of the sites. The initial contact angle on control sample C1 (99 – 108°) was slightly smaller than those on photocatalytic samples P1 (108 – 123°) and P2 (107 – 114°). Initial contact angles of control and photocatalytic samples in our study were significantly higher than those reported for photocatalytic limestone surfaces (40°) and their corresponding uncoated controls (55°) as reported in a recent study [54]. This significant difference in contact angle among different types of products may result from the more hydrophobic nature of fluorinated polymeric matrices (including those from our study), as compared with limestone.

The small difference in contact angle between control and photocatalytic materials observed in our study may correspond to the presence of TiO_2 additives or changes in the surface morphology in P1 and P2. The overall range of contact angle values measured for both control and photocatalytic samples was consistent with those measured in TiO_2-coated polymer used in cool roofing materials, which increased to 103° from 86° (uncoated polymer) upon coating with TiO_2 [71]. However, not all TiO_2-modified polymers reported in the literature show the same trend. On another study, addition of TiO_2 nanoparticles to a more hydrophobic polymer building coating (initial water contact angle approximately 125°) decreased the contact angle of unexposed specimens by 15-25° [23]. Such difference with the control material was retained after one year of exposure in an urban environment.

In two of the three sites, the control sample C1 showed a significant reduction in contact angle after two years of exposure, reaching an average of 81° in Berkeley, and an average of 85° in Fresno. Such reduction in contact angle on the non-photocatalytic sample is consistent with similar trends reported in the literature for limestone [54] and polymeric coatings [23]. These may be associated with buildup of soiling materials, some of which may contribute to surface

hydrophilicity (e.g., salts or organic acids). Contact angles measured in the P1 and P2 samples did not show a significant change after two years of exposure. Those aged samples remained within ±6°, on average, with respect to the contact angle of unexposed (pre-bleached) specimens. This result agrees with another report in the literature showing small changes in surface hydrophilicity of photocatalytic building coatings subjected to accelerated climatic aging [72]. By contrast, field aging of TiO_2-modified polymeric coatings showed a significant decrease in contact angle values after one year of field exposure in an urban setting [23]. The small contact angle changes observed in aged samples P1 and P2 on our study are consistent with the limited accumulation of atmospheric deposition and soiling material on these photocatalytic surfaces. These small changes in contact angle are consistent with the negligible changes observed in albedo, as described below.

Some photocatalytic materials are known to become more hydrophilic under irradiation, through photoinduced superhydrophilicity, with liquid water films facilitating the self-cleaning effect by mechanical removal of particles and adsorbates from the surface [36-38]. However, contact angle measurements in this study were performed in the absence of UV illumination, and for that reason these tests did not explore the contribution of photoinduced hydrophilicity to self-cleaning properties. The goal of these measurements, instead, was to assess changes in hydrophilicity at the catalyst surface, primarily due to atmospheric deposition. Other possible chemical changes could be attributed to material degradation, leading to the possible photocatalyst loss over the exposure period, but SEM-EDS analysis of the surface prior and after exposure showed that the content of TiO_2 was retained over the two-year field aging period (as described in Section 3.2.2, below).

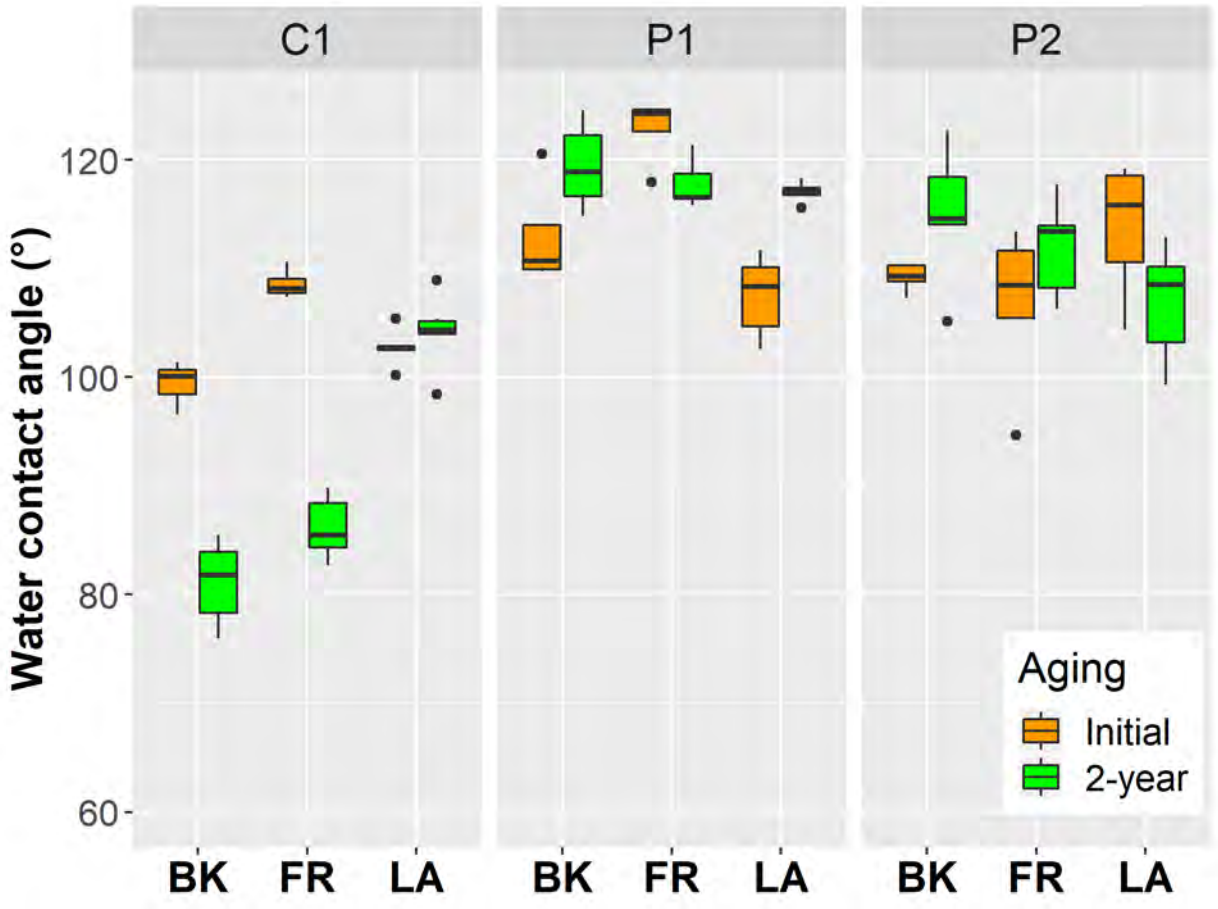

Figure 3. Water contact angles measured before and after two years of natural exposure in three California sites. The central line in each boxplot represents the median of six measurements, and the top and bottom of the box the two central quartiles. Highest and lowest values in the distribution are shown with whiskers, except for outliers falling beyond 1.5 times the interquartile range, IQR (black circles).

3.2.2 Microscopic analysis

The chemical nature and morphology of soiling particles was assessed by SEM-EDS. Analyses included specimens from the three samples (C1, P1 and P2), exposed at the three locations after six months of exposure. These corresponded to the highest level of soiling over the entire study period. Microscope images of 1 mm by 1 mm regions on each specimen's surface are shown in Figure 4. In each case, the images are a good representation of the whole sample. The background in all images corresponds to the fluorinated polymer coating applied to the fiberglass fibers of the architectural membrane, which in the case of P1 and P2 was functionalized with photocatalytic TiO_2. Cracks shown on the polymer are not related to exposure in the environment. These are features present in the unexposed material, as shown in Figure S3 (Supporting Information).

Particle deposition on specimens of control sample C1 was greater in Fresno than in Los Angeles. By contrast, those exposed in Berkeley were the cleanest. In each of the exposure sites, images of the two photocatalytic samples P1 and P2 showed less soiling than those of the control sample C1. These results are consistent with visual inspection of the specimens and with albedo measurements.

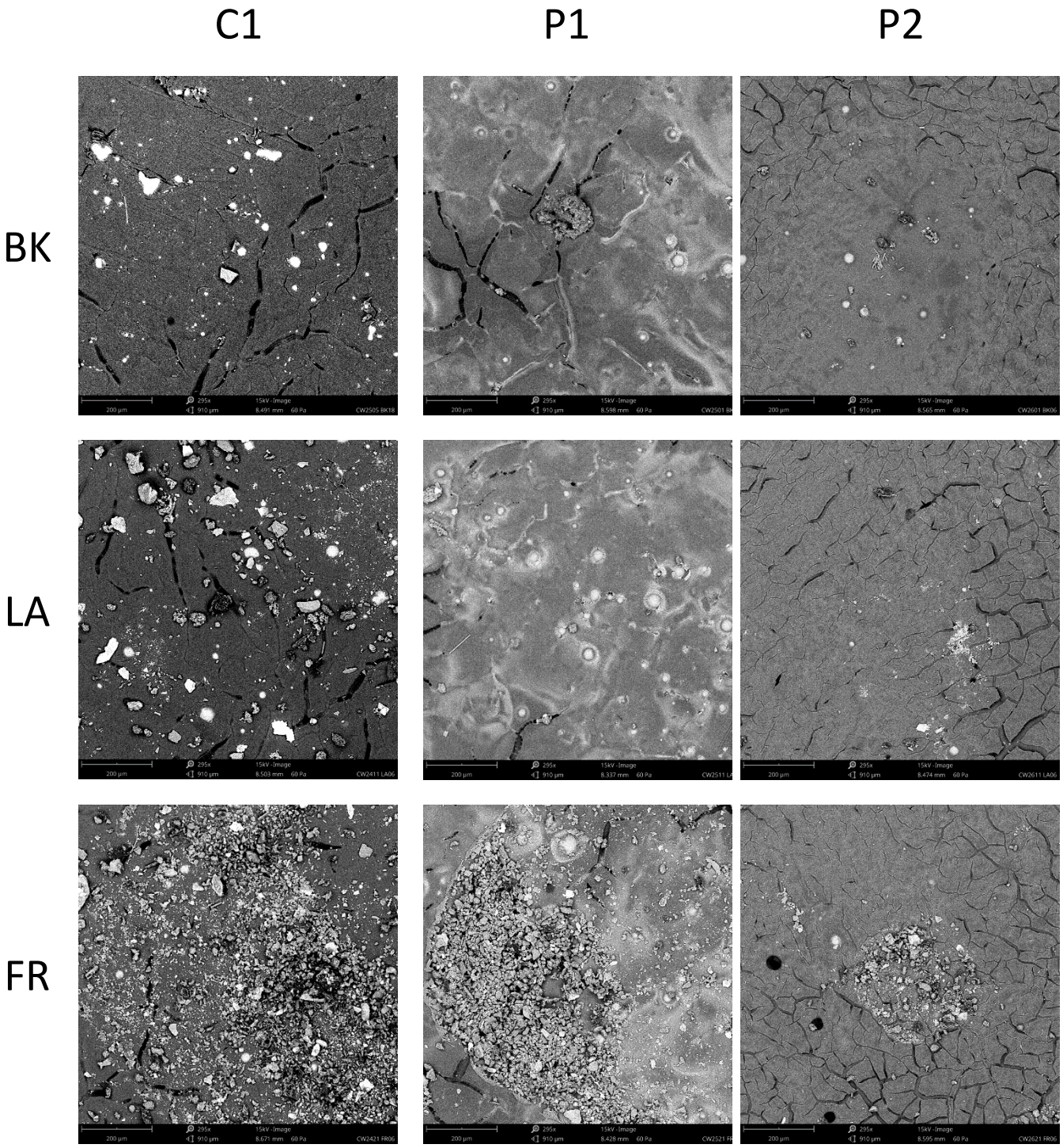

Figure 4. SEM images of C1 (control), P1 and P2 samples after six months of exposure at the Berkeley (BK), Los Angeles (LA), and Fresno (FR) sites, showing soiling particles deposited on the surface. Image magnification: 295x. Image size: 1 mm by 1mm.

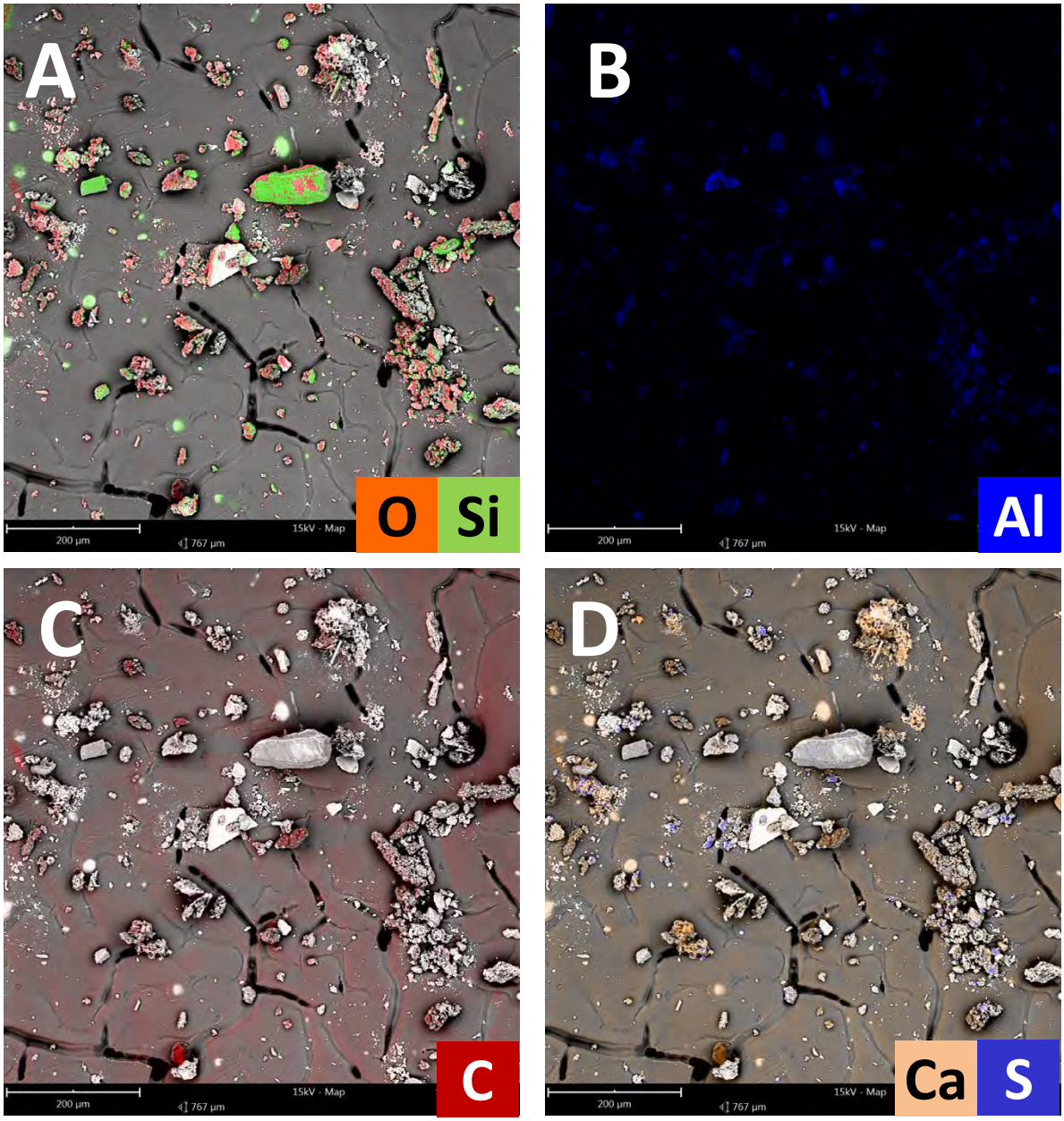

Figure 5. SEM-EDS surface map of a C1 sample exposed in Los Angeles for six months. The soiling is mostly composed of alumino-silicates, with particles containing (A) oxygen and silicon; (B) aluminum, (C) carbon (soot); and (D) calcium and sulfur. Small amounts of phosphorus and nitrogen were also found in some samples (not shown).

Analysis by SEM-EDS permitted a qualitative chemical characterization of soiling particles, illustrated in Figure 5 for sample C1 after six months of exposure in Los Angeles. Additional evidence is also presented as Supporting Information in Figure S4 (full SEM image) and Figure S5 (surface map of soiling constituents). Elemental constituents of soiling particles included oxygen, silicon, aluminum, carbon, calcium, sulfur, phosphorus and nitrogen. Larger particles were primarily silica and alumino-silicates (Figure 5a and 5b). Carbon-containing particles were often associated with calcium (Figure 5c and 5d). The carbon content is likely attributed to soot particles. Sulfur was found in small aggregates (Figure 5d). Phosphorus and nitrogen (not shown in Figure 5) were found occasionally in small quantities. This qualitative identification of several elements confirmed the presence of common soiling constituents that had previously been reported, including black carbon (soot), mineral dust (metal oxides, clays), inorganic salts (containing Na^+, Ca^{2+}, Cl^- and SO_4^{2-} as main ionic constituents) and organic matter [73]. This analysis does not allow for a quantitative comparison between different locations, or between photocatalytic and control materials, which showed presence of similar chemical species.

SEM-EDS analysis was also used to quantify Ti in unexposed and two-year exposed specimens, to assess potential catalyst losses due to material weathering upon exposure to the environment. It was observed that the amount of Ti remaining on the surface after 2 years in the field was 95% ± 10% for P1, and 112% ± 10% for P2. These results suggest that there was no significant catalyst loss during the two-year exposure period, consistent with findings from field testing [56] and laboratory accelerated testing [55]. While those studies were carried out using other photocatalytic construction (cementitious) materials, one common characteristic is that TiO_2 additives were embedded in the material (rather than adsorbed as a coating), providing greater durability.

3.3 Evaluation of the self-cleaning effect

3.3.1 Visual inspection

The self-cleaning effect was visible to the naked eye, as illustrated in Figure 6 for specimens exposed in Fresno. Images from the other two sites show the same trends. Specimens of C1

were much more soiled than those of P1 and P2, leading to appreciable darkening and formation of dust and particle clusters. This effect was more marked during the dry season and was significantly reduced during the rainy season. The effect was also stronger in specimens exposed in Los Angeles and Fresno, with respect to those aged in Berkeley.

3.3.2 Albedo measurements

Measurements of albedo as a function of exposure time confirmed that when the white control sample C1 became dirtier, its albedo was reduced. Figure 7 compares, for each of the three sites, the albedo recorded for the control sample C1 with that measured on the photocatalytic samples P1 and P2. Both photocatalytic products showed a remarkable retention of the initial albedo over the two-year study period in the three exposure sites, with minimal changes that were in most cases of the same magnitude as the experimental error. For sample P1, the average albedo comprising all specimens measured over two years was 0.745 ± 0.003 (BK), 0.741 ± 0.005 (LA) and 0.740 ± 0.006 (FR), compared with the initial measurement of 0.743 ± 0.001. Similarly, for sample P2 it was 0.752 ± 0.006 (BK), 0.745 ± 0.007 (LA) and 0.746 ± 0.010 (FR), compared with the initial measurement of 0.747 ± 0.002.

Results obtained for each site showed that specimens exposed in Los Angeles and Fresno were more affected by soiling than those exposed in Berkeley. This is due to the presence of stronger sources of atmospheric pollution in the proximity of the materials, as evidenced by higher $PM_{2.5}$ levels during the dry season at those sites. All three sites showed seasonal variations in the albedo of the control specimen C1, falling during the dry season and rising during the rainy season. The largest albedo difference (photocatalytic material minus control material) was 0.10, and was observed in Los Angeles and Fresno during the summer of 2016. The gap between the albedo of photocatalytic and control materials was reduced during the rainy season, due to the cleaning of the control material by rain, which brought the albedo of the C1 specimens to values closer to those from the P1 and P2 specimens.

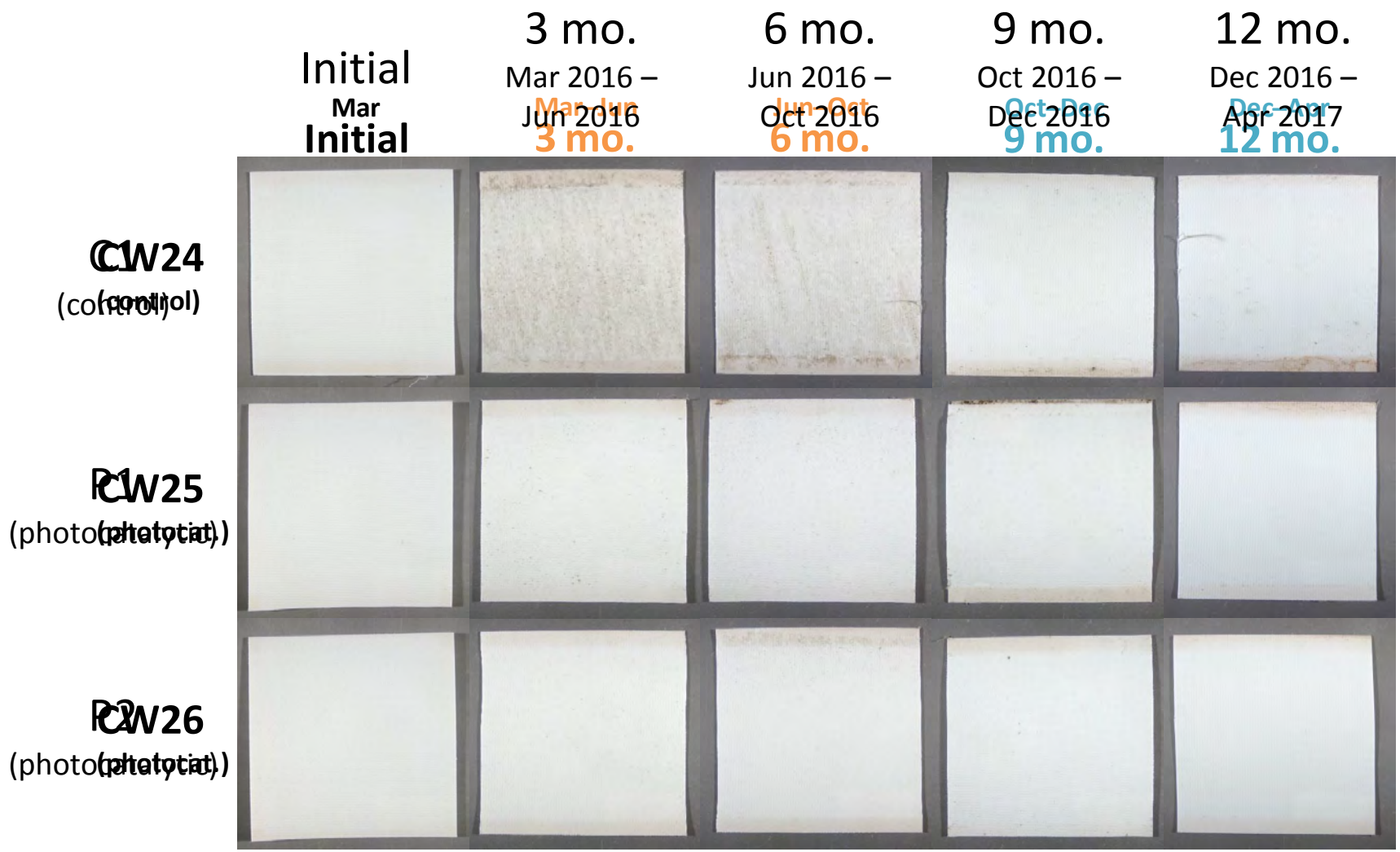

Figure 6. Images of specimens exposed at the Fresno site**.** Image size: 10 cm by 10 cm.

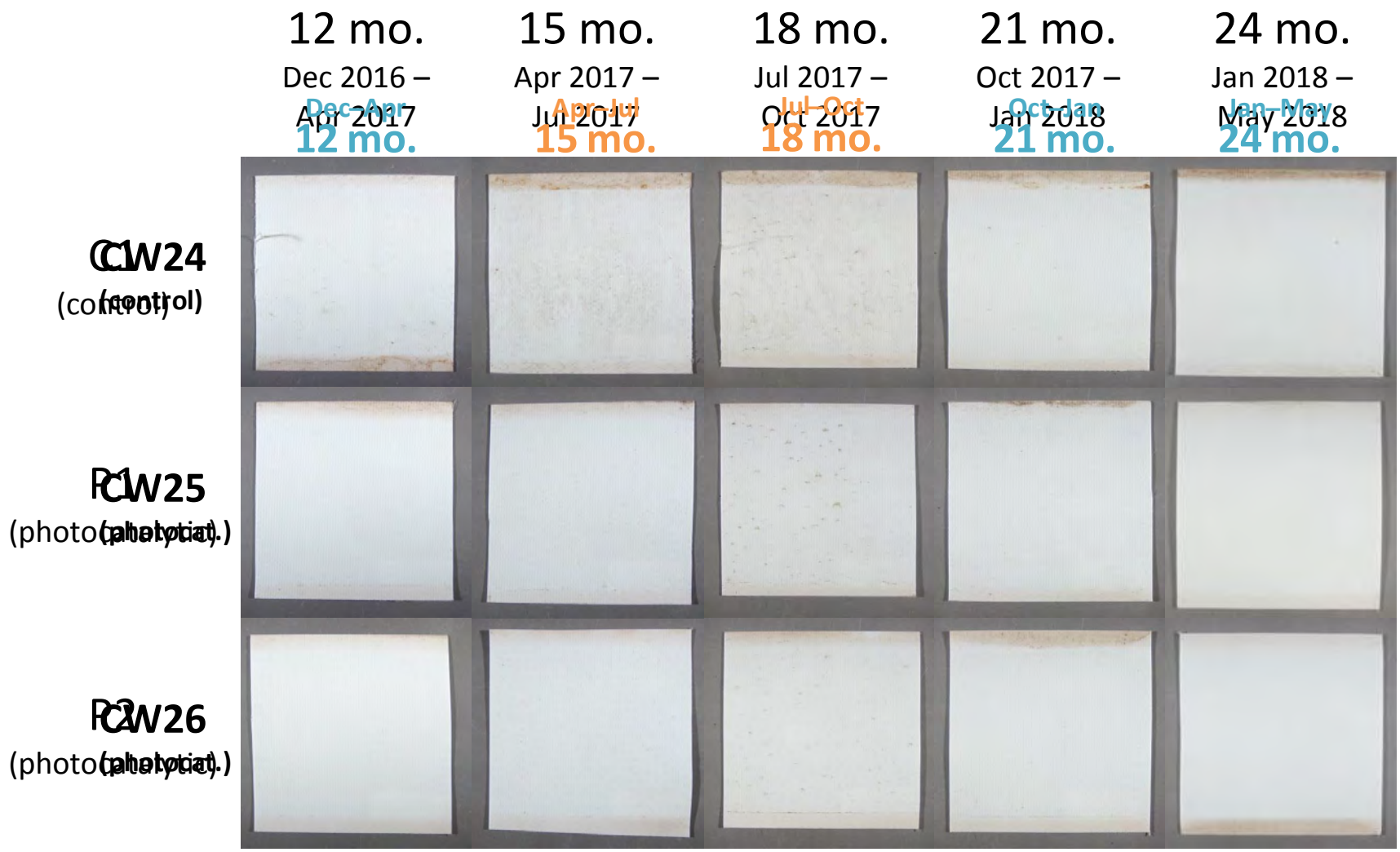

Figure 6. (Cont'd).

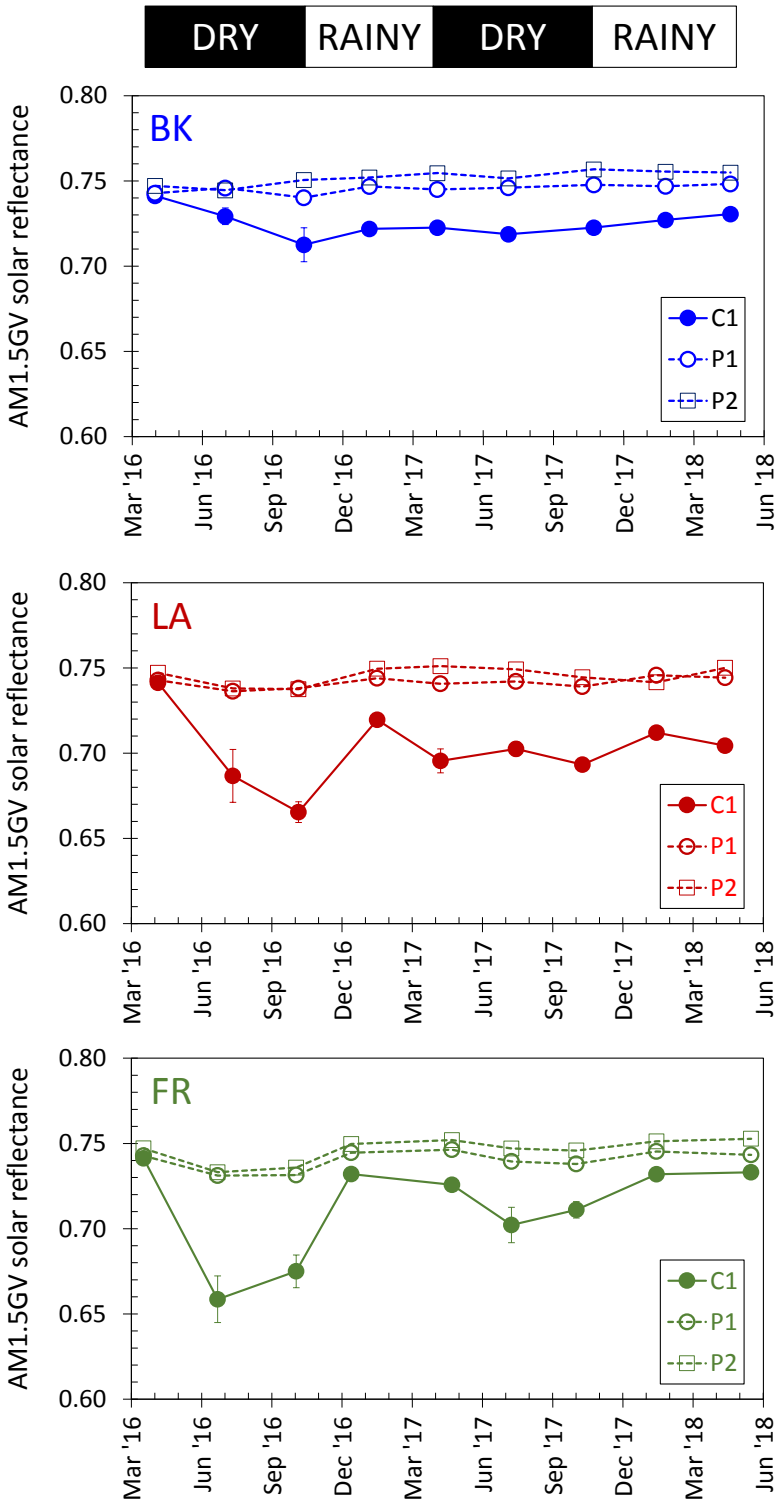

Figure 7. Air mass 1.5 global vertical (sun-facing) solar reflectance (albedo) of architectural fabric C1 (control) vs. samples P1 and P2 (photocatalytic) measured in the Berkeley (BK), Los Angeles (LA), and Fresno (FR) sites.

3.4 Evaluation of the de-pollution effect

3.4.1 NO and NO_2 concentration profiles

Figure S1 (Supplemental Information) illustrates experimental results obtained in a typical experiment carried out to evaluate the NO_x removal efficiency of the photocatalytic specimens and the control material. On the x-axis, t = 0 corresponds to the time at which the UV lamp was turned on. Before the UV lamp was turned on, the material reached equilibrium with the NO-enriched atmosphere in the dark. When the control specimen C1 was used, no changes in NO and NO_2 concentrations were observed under UV light, indicating that there was no reaction taking place upon irradiation alone (Figure S1-A). However, when specimens from the materials P1 and P2 were used, the NO and NO_2 curves showed features similar to those presented in Figure S1-B. There was an initial sharp decline in NO concentrations, accompanied by an increase in NO_2 concentrations. Subsequently, NO concentrations increased asymptotically reaching a steady-state value after about 3 h of irradiation. During the same period, NO_2 concentrations declined reaching a plateau at the same time. After six hours of irradiation, the UV lamp was turned off, and both NO and NO_2 concentrations rapidly recovered their initial values (ca. 1000 ppb and 0 ppm, respectively). Measurements continued during approximately 1 h in the dark, to establish final equilibrium conditions.

3.4.2 NO removal rates

From the integration of the curves shown in Figure S1, the rate of NO elimination was calculated using Eqs. (1) and (2). The NO removal rate is reported in Figure 8 for P1 and P2 specimens as a function of the exposure duration. The elimination of NO was the primary photocatalytic process, which led to the formation of NO_2 and nitrate [74-77]. The P1 sample showed a significantly higher NO elimination efficiency with respect to P2 in all three sites and almost all weather conditions. Based on the results presented in Figure 8, the photocatalytic activity of product P1 declined in all three sites during the dry season. This is likely due to deposition and attachment of soiling agents onto the catalyst surface. Specimens exposed in Berkeley and Fresno recovered their photocatalytic activity after a year of exposure, at the end

of the first rainy season. In Berkeley, the recovered activity exceeded the initial performance of unexposed materials. This may have resulted from additional activation of the catalyst upon environmental exposure over time. This activation could be caused by the removal of surface coatings remaining from the manufacturing process, or by abrasion of the polymer matrix, either of which could expose more catalyst particles. By contrast, the albedos of specimens exposed in Los Angeles did not increase during the rainy season. This is likely due to less rain in Los Angeles, and may also reflect the fact that the chemical nature of soiling in all three sites is different. In the case of sample P2, NO removal rates were lower, but still showed some of the same seasonal effects. For sample P2, specimens exposed in Fresno that were retrieved during the dry season showed negative values of the NO removal rate, as NO concentrations downstream of the test chamber were slightly higher than those measured upstream in the challenge gas. This effect can be attributed to the possible presence of ammonium salts, and possibly other reduced nitrogen contaminants, as part of the soiling mixture deposited on the specimen surface. The photocatalytic oxidation of these species has been shown to produce both NO and NO_2 [78].

3.4.3 NO_x deposition rates

By subtracting the NO_2 formation rate from the NO removal rate, it was possible to determine in each case the NO_x deposition rate, which is presented in Figure 9 for both photocatalytic samples. Overall, the NO_x deposition rate was slower than the NO removal rate (primary photocatalytic process), because a large fraction of NO was converted to NO_2, and did not contribute to NO_x elimination. However, there was a net NO_x deposition rate in most conditions. Similar to trends described above for NO removal, sample P1 was more effective in the deposition of NO_x than sample P2. The P1 sample showed positive values for the NO_x deposition rate for specimens exposed in all three sites over the entire exposure period, except for one specimen in Fresno. In some cases, the NO_x deposition rate of aged materials was higher than that determined for unexposed samples, owing to catalyst activation and soiling removal as described above. The P2 sample showed negative NO_x deposition rates in Fresno over the whole exposure period. In addition, a few specimens exposed in Los Angeles also had

423 negative values. As described above, these negative values represent higher downstream than
424 upstream concentrations, which can be attributed to the photocatalytic oxidation of nitrogen-
425 containing species in soiling material deposited on the specimens. This is particularly relevant
426 for ammonia aerosols, which are commonly found in rural environments with agricultural
427 activities such as the one surrounding the Fresno site [79].

428 While the photocatalytic materials were very effective in preventing albedo losses by removing
429 soiling agents that could be visualized with the naked eye and microscopy tools, it is likely that
430 some recalcitrant oxidation byproducts can remain attached to the catalyst and build up over
431 time during the dry season. Examples of those recalcitrant species are carboxylic and
432 polycarboxylic acids, which have a low vapor pressure and can attach to active sites, thus
433 partially inhibiting the catalysts ability to react with NO_x and other atmospheric species [80-82].
434 Similarly, inorganic species such as soluble salts formed as byproducts of the photocatalytic
435 process or present in atmospheric deposition could deactivate the catalyst [53, 54, 77]. This
436 effect can be reduced during the rainy season because, while those species are not volatile,
437 they are water soluble and can be dissolved and removed by liquid water present on the
438 surface.

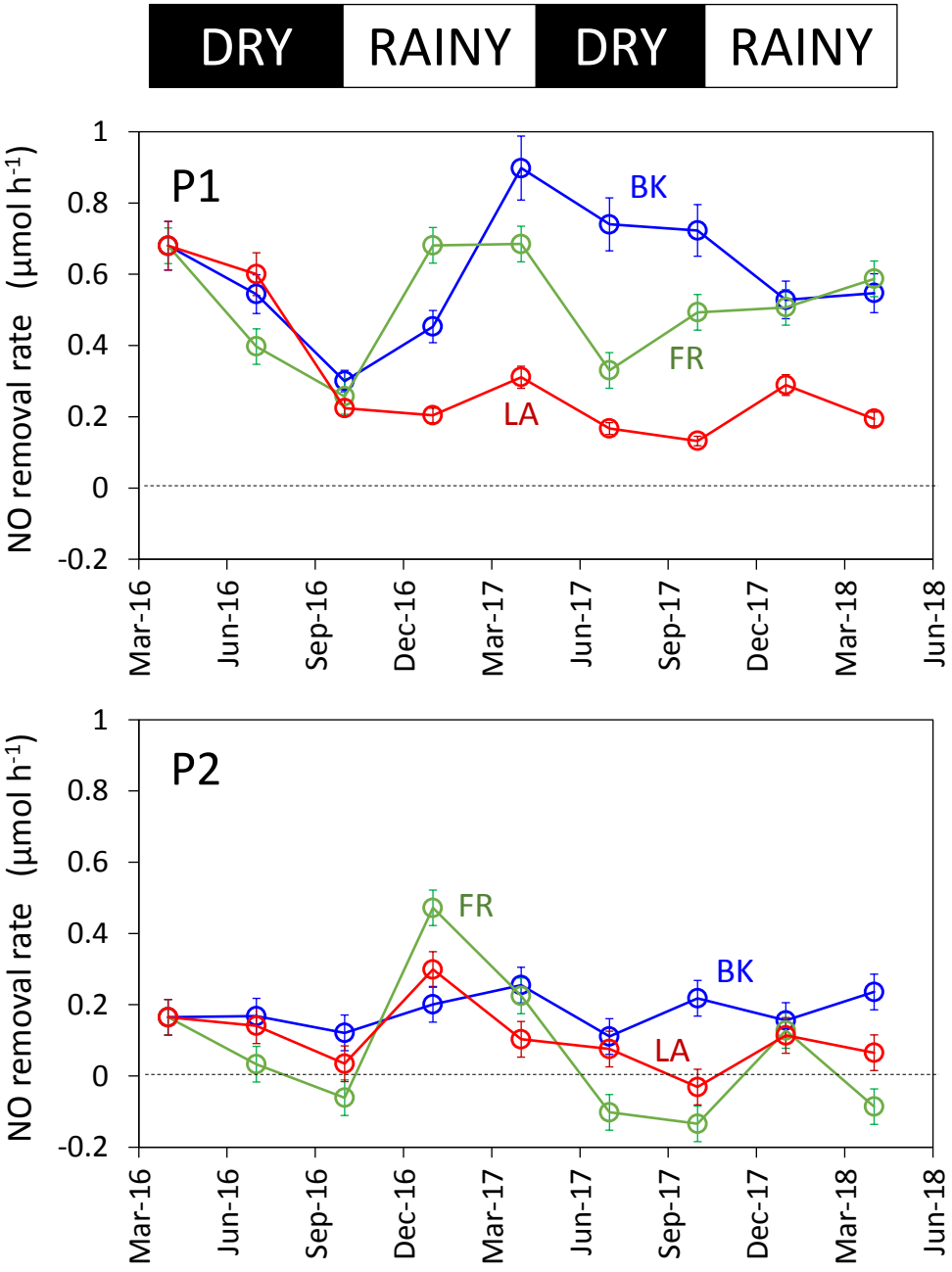

Figure 8. Laboratory-measured rates of NO removal by photocatalytic samples P1 and P2 exposed in Berkeley (BK), Los Angeles (LA), and Fresno (FR). The control sample C1 did not catalyze the elimination of NO.

447

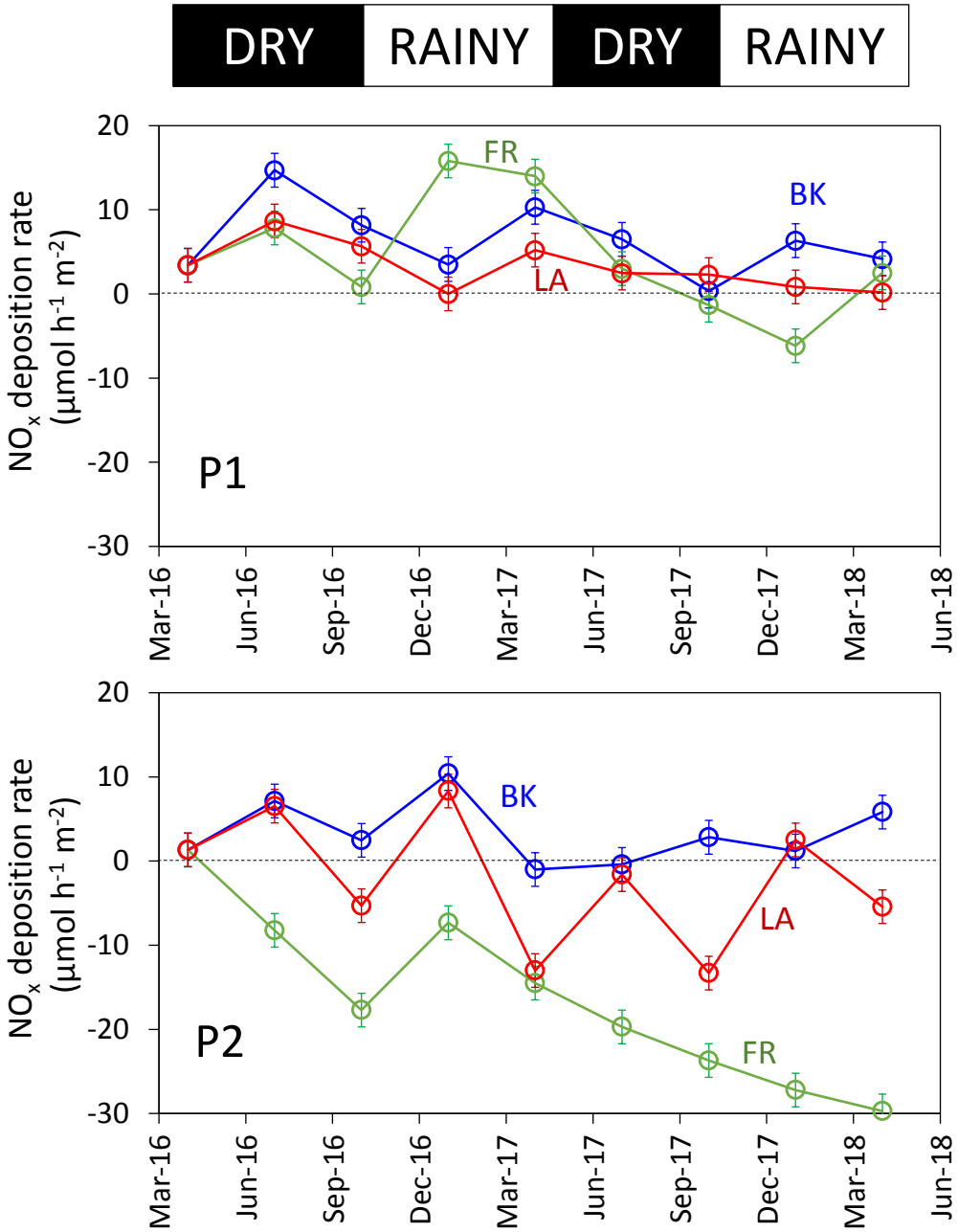

448

449

450 **Figure 9. Laboratory-determined** NO_x deposition rate over photocatalytic samples P1 and P2, exposed
451 at the Berkeley (BK), Los Angeles (LA), and Fresno (FR) sites. The control sample C1 did not catalyze
452 the elimination of NO_x.

453

4 Conclusions

This study illustrated the performance of advanced building materials under realistic conditions over a long enough duration to assess initial changes and seasonal effects. The materials were exposed in three different sites with different levels and chemical composition of atmospheric pollution. Both photocatalytic products (P1 and P2) showed an excellent self-cleaning performance in all three California sites and during all seasons. The photocatalyst additives can successfully protect the surface from soiling buildup, preserving its original appearance and energy benefits.

By contrast, the de-pollution effect showed a marked effect of both the exposure location and weather. The de-pollution capacity of sample P1 was significantly higher than that of sample P2, illustrating the critical role of product formulation in achieving the desired performance. These results suggest that photocatalytic materials can achieve good self-cleaning results even in cases in which they have limited capacity for atmospheric de-pollution. While NO removal and a net NO_x deposition were observed in most cases, there were fluctuations that were associated with the effects of atmospheric deposition (partial inhibition) and precipitation (re-activation).

Future work should explore the effects of other climate and pollution conditions different from those found in California, and durability of the photocatalyst performance over longer periods. Other photocatalytic building materials should also be assessed under realistic exposure conditions over long periods of time, such as those reported here.

Acknowledgement

This research was supported by the California Energy Commission under contract EPC-14-010. This work was also supported by the Assistant Secretary for Energy Efficiency and Renewable Energy, Building Technologies Office of the U.S. Department of Energy under Contract No. DE-

AC02-05CH11231. The authors thank David Speiser (industrial partner) and Trevor Krasowsky (University of Southern California) for assistance in specimen exposure and retrieval.

References

[1] A.H. Rosenfeld, H. Akbari, J.J. Romm, M. Pomerantz, Cool communities: strategies for heat island mitigation and smog reduction, Energy and Buildings 28 (1998) 51-62. 10.1016/s0378-7788(97)00063-7

[2] H. Akbari, R. Levinson, L. Rainer, Monitoring the energy-use effects of cool roofs on California commercial buildings, Energy and Buildings 37 (2005) 1007-1016. 10.1016/j.enbuild.2004.11.013

[3] R. Levinson, H. Akbari, Potential benefits of cool roofs on commercial buildings: conserving energy, saving money, and reducing emission of greenhouse gases and air pollutants, Energy Efficiency 3 (2009) 53-109. 10.1007/s12053-008-9038-2

[4] A.L. Pisello, F. Cotana, The thermal effect of an innovative cool roof on residential buildings in Italy: Results from two years of continuous monitoring, Energy and Buildings 69 (2014) 154-164. 10.1016/j.enbuild.2013.10.031

[5] P.J. Rosado, D. Faulkner, D.P. Sullivan, R. Levinson, Measured temperature reductions and energy savings from a cool tile roof on a central California home, Energy and Buildings 80 (2014) 57-71. 10.1016/j.enbuild.2014.04.024

[6] A. Synnefa, M. Santamouris, H. Akbari, Estimating the effect of using cool coatings on energy loads and thermal comfort in residential buildings in various climatic conditions, Energy and Buildings 39 (2007) 1167-1174. 10.1016/j.enbuild.2007.01.004

[7] R.M. Levinson, H.E. Gilbert, J. Zhang, G. Ban-Weiss, J. Kleissl, M. Pizzicotti, W. Zhang, N. Dumas, B. Kurtz, Y. Long, N. Nazarian, A. Mohegh, Y. Li, X. Tang, S.S. Chen, M.L. Russell, S. Houzé

503 de l'Aulnoit, P. Berdahl, P. Rosado, J. Slack, H. Goudy, H. Destaillats, Solar-Reflective "Cool"
504 Walls: Benefits, Technologies, and Implementation, (2019).
505 https://www.energy.ca.gov/2019publications/CEC-500-2019-040/

506 [8] P.J. Rosado, R. Levinson, Potential benefits of cool walls on residential and commercial
507 buildings across California and the United States: Conserving energy, saving money, and
508 reducing emission of greenhouse gases and air pollutants, Energy and Buildings 199 (2019) 588-
509 607. 10.1016/j.enbuild.2019.02.028

510 [9] H. Akbari, M. Pomerantz, H. Taha, Cool surfaces and shade trees to reduce energy use and
511 improve air quality in urban areas, Solar Energy 70 (2001) 295-310. 10.1016/s0038-
512 092x(00)00089-x

513 [10] D. Millstein, S. Menon, Regional climate consequences of large-scale cool roof and
514 photovoltaic array deployment, Environmental Research Letters 6 (2011) 034001.
515 10.1088/1748-9326/6/3/034001

516 [11] K.W. Oleson, G.B. Bonan, J. Feddema, Effects of white roofs on urban temperature in a
517 global climate model, Geophysical Research Letters 37 (2010) L03701. 10.1029/2009GL042194

518 [12] M. Santamouris, Cooling the cities – A review of reflective and green roof mitigation
519 technologies to fight heat island and improve comfort in urban environments, Solar Energy 103
520 (2014) 682-703. 10.1016/j.solener.2012.07.003

521 [13] H. Akbari, H. Damon Matthews, D. Seto, The long-term effect of increasing the albedo of
522 urban areas, Environmental Research Letters 7 (2012) 024004. 10.1088/1748-9326/7/2/024004

523 [14] R. Paolini, A. Zani, T. Poli, F. Antretter, M. Zinzi, Natural aging of cool walls: Impact on
524 solar reflectance, sensitivity to thermal shocks and building energy needs, Energy and Buildings
525 153 (2017) 287-296. 10.1016/j.enbuild.2017.08.017

526 [15] R.M. Levinson, P.H. Berdahl, A.A. Berhe, H. Akbari, Effects of soiling and cleaning on the
527 reflectance and solar heat gain of a light-colored roofing membrane, Atmos. Environ. 39 (2005)
528 7807-7824. 10.1016/j.atmosenv.2005.08.037

529 [16] P.H. Berdahl, H. Akbari, L.S. Rose, Aging of reflective roofs: soot deposition, Applied
530 Optics 41 (2002) 2355-2360. 10.1364/ao.41.002355

531 [17] S.E. Bretz, H. Akbari, Long-term performance of high-albedo roof coatings, Energy and
532 Buildings 25 (1997) 159-167. 10.1016/s0378-7788(96)01005-5

533 [18] C. Ferrari, A. Gholizadeh Touchaei, M. Sleiman, A. Libbra, A. Muscio, C. Siligardi, H.
534 Akbari, Effect of aging processes on solar reflectivity of clay roof tiles, Advances in Building
535 Energy Research 8 (2014) 28-40. 10.1080/17512549.2014.890535

536 [19] M. Sleiman, G. Ban-Weiss, H.E. Gilbert, D. François, P. Berdahl, T.W. Kirchstetter, H.
537 Destaillats, R. Levinson, Soiling of building envelope surfaces and its effect on solar
538 reflectance—Part I: Analysis of roofing product databases, Solar Energy Materials and Solar
539 Cells 95 (2011) 3385-3399. 10.1016/j.solmat.2011.08.002

540 [20] M.V. Diamanti, M. Ormellese, M.P. Pedeferri, Characterization of photocatalytic and
541 superhydrophilic properties of mortars containing titanium dioxide, Cement and Concrete
542 Research 38 (2008) 1349-1353. 10.1016/j.cemconres.2008.07.003

543 [21] A. Folli, C. Pade, T.B. Hansen, T. De Marco, D.E. Macphee, TiO_2 photocatalysis in
544 cementitious systems: Insights into self-cleaning and depollution chemistry, Cement and
545 Concrete Research 42 (2012) 539-548. 10.1016/j.cemconres.2011.12.001

546 [22] G.L. Guerrini, Photocatalytic performances in a city tunnel in Rome: NO_x monitoring
547 results, Construction and Building Materials 27 (2012) 165-175.
548 10.1016/j.conbuildmat.2011.07.065

549 [23] D. Colangiuli, M. Lettieri, M. Masieri, A. Calia, Field study in an urban environment of
550 simultaneous self-cleaning and hydrophobic nanosized TiO_2-based coatings on stone for the
551 protection of building surface, Science of the Total Environment 650 (2019) 2919-2930.
552 10.1016/j.scitotenv.2018.10.044

553 [24] Greenbiz.com-Buildings, Alcoa develops smog-eating panels to keep building clean
554 (2011), Reuters (Accessed on: May 13, 2020).
555 https://www.reuters.com/article/idUS291593569120110509

556 [25] Sheerfill, EverClean(R) Technology (2020), Saint Gobain (Accessed on: May 13, 2020).
557 https://www.sheerfill.com/everclean-technology

558 [26] X. Tang, L. Ughetta, S.K. Shannon, S. Houzé de l'Aulnoit, S.S. Chen, R.A.T. Gould, M.L.
559 Russell, J. Zhang, G. Ban-Weiss, R.L.A. Everman, F.W. Klink, R.M. Levinson, H. Destaillats, De-
560 pollution efficacy of photocatalytic roofing granules, Build Environ 160 (2019) 106058.
561 10.1016/j.buildenv.2019.03.056

562 [27] M. Gagliardi, Photocatalysts: Technology and Global Markets (2015), BCC Research,
563 (Accessed on: May 13, 2020). https://www.bccresearch.com/market-research/advanced-
564 materials/photocatalysts-technologies-markets-report-avm069b.html

565 [28] M.V. Diamanti, B. Del Curto, M. Ormellese, M.P. Pedeferri, Photocatalytic and self-
566 cleaning activity of colored mortars containing TiO_2, Construction and Building Materials 46
567 (2013) 167-174. 10.1016/j.conbuildmat.2013.04.038

568 [29] K. Guan, Relationship between photocatalytic activity, hydrophilicity and self-cleaning
569 effect of TiO_2/SiO_2 films, Surface and Coatings Technology 191 (2005) 155-160.
570 10.1016/j.surfcoat.2004.02.022

571 [30] S.-K. Lee, S. McIntyre, A. Mills, Visible illustration of the direct, lateral and remote
572 photocatalytic destruction of soot by titania, Journal of Photochemistry and Photobiology A:
573 Chemistry 162 (2004) 203-206. 10.1016/j.nainr.2003.07.002

574 [31] A. Mills, S. Hodgen, S.K. Lee, Self-cleaning titania films: an overview of direct, lateral and
575 remote photo-oxidation processes, Research on Chemical Intermediates 31 (2005) 295-308.
576 10.1163/1568567053956644

577 [32] M. Janus, J. Zatorska, A. Czyżewski, K. Bubacz, E. Kusiak-Nejman, A.W. Morawski, Self-
578 cleaning properties of cement plates loaded with N,C-modified TiO_2 photocatalysts, Applied
579 Surface Science 330 (2015) 200-206. 10.1016/j.apsusc.2014.12.113

580 [33] E. Jimenez-Relinque, J.R. Rodriguez-Garcia, A. Castillo, M. Castellote, Characteristics and
581 efficiency of photocatalytic cementitious materials: Type of binder, roughness and
582 microstructure, Cement and Concrete Research 71 (2015) 124-131.
583 10.1016/j.cemconres.2015.02.003

584 [34] ISO Standard 10678. Fine ceramics (advanced ceramics, advanced technical ceramics) —
585 Determination of photocatalytic activity of surfaces in an aqueous medium by degradation of
586 methylene blue, International Organization for Standardization (2010).
587 https://www.iso.org/standard/46019.html

588 [35] UNI Standard 11259:2008. Determination of the photocatalytic activity of hydraulic
589 binders. Rodammina test method, Ente Nazionale Italiano di Unificazione (2008).
590 https://infostore.saiglobal.com/en-us/standards/uni-11259-2008-
591 1071923_saig_uni_uni_2498224/

592 [36] S. Banerjee, D.D. Dionysiou, S.C. Pillai, Self-cleaning applications of TiO_2 by photo-
593 induced hydrophilicity and photocatalysis, Applied Catalysis B: Environmental 176-177 (2015)
594 396-428. 10.1016/j.apcatb.2015.03.058

595 [37] D. Ollis, Connecting contact angle evolution to photocatalytic kinetics of self cleaning
596 surfaces, Catal Today 310 (2018) 49-58. 10.1016/j.cattod.2017.09.051

[38] Y. Yin, T. Li, F. Fan, C. Zhao, C. Wang, Dynamically modifiable wettability comparisons of the hydrophilic and hydrophobic substrates coated with F/TiO_2 hybrid sol by UV irradiation, Applied Surface Science 283 (2013) 482-489. 10.1016/j.apsusc.2013.06.133

[39] ISO Standard 27448. Fine ceramics (advanced ceramics, advanced technical ceramics) — Test method for self-cleaning performance of semiconducting photocatalytic materials — Measurement of water contact angle, International Organization for Standardization (2009). https://www.iso.org/standard/53953.html

[40] A.H. Aïssa, E. Puzenat, A. Plassais, J.-M. Herrmann, C. Haehnel, C. Guillard, Characterization and photocatalytic performance in air of cementitious materials containing TiO_2. Case study of formaldehyde removal, Applied Catalysis B: Environmental 107 (2011) 1-8. 10.1016/j.apcatb.2011.06.012

[41] A. Strini, S. Cassese, L. Schiavi, Measurement of benzene, toluene, ethylbenzene and o-xylene gas phase photodegradation by titanium dioxide dispersed in cementitious materials using a mixed flow reactor, Applied Catalysis B: Environmental 61 (2005) 90-97. 10.1016/j.apcatb.2005.04.009

[42] A. Strini, L. Schiavi, Low irradiance toluene degradation activity of a cementitious photocatalytic material measured at constant pollutant concentration by a successive approximation method, Applied Catalysis B: Environmental 103 (2011) 226-231. 10.1016/j.apcatb.2011.01.031

[43] M. Hunger, G. Hüsken, H.J.H. Brouwers, Photocatalytic degradation of air pollutants — From modeling to large scale application, Cement and Concrete Research 40 (2010) 313-320. 10.1016/j.cemconres.2009.09.013

[44] R. Dillert, J. Stotzner, A. Engel, D.W. Bahnemann, Influence of inlet concentration and light intensity on the photocatalytic oxidation of nitrogen(II) oxide at the surface of Aeroxide(R) TiO_2 P25, J Hazard Mater 211-212 (2012) 240-246. 10.1016/j.jhazmat.2011.11.041

622 [45] A. Mills, C. Hill, P.K.J. Robertson, Overview of the current ISO tests for photocatalytic
623 materials, Journal of Photochemistry and Photobiology A: Chemistry 237 (2012) 7-23.
624 10.1016/j.jphotochem.2012.02.024

625 [46] C. Minero, A. Bedini, M. Minella, On the Standardization of the Photocatalytic Gas/Solid
626 Tests, International Journal of Chemical Reactor Engineering 11 (2013) 717. 10.1515/ijcre-2012-
627 0045

628 [47] ISO Standard 22197-1. Fine ceramics (advanced ceramics, advanced technical ceramics)
629 – test method for air-purification performance of semiconducting photocatalytic materials.
630 Part 1. Removal of nitric oxide, International Organization for Standardization (2007).
631 https://www.iso.org/standard/65416.html

632 [48] Q.L. Yu, Y. Hendrix, S. Lorencik, H.J.H. Brouwers, Field study of NO_x degradation by a
633 mineral-based air purifying paint, Build Environ 142 (2018) 70-82.
634 10.1016/j.buildenv.2018.06.014

635 [49] M.M. Ballari, H.J.H. Brouwers, Full scale demonstration of air-purifying pavement, J
636 Hazard Mater 254-255 (2013) 406-414. 10.1016/j.jhazmat.2013.02.012

637 [50] A. Folli, M. Strøm, T.P. Madsen, T. Henriksen, J. Lang, J. Emenius, T. Klevebrant, Å.
638 Nilsson, Field study of air purifying paving elements containing TiO_2, Atmos. Environ. 107 (2015)
639 44-51. 10.1016/j.atmosenv.2015.02.025

640 [51] M. Gallus, V. Akylas, F. Barmpas, A. Beeldens, E. Boonen, A. Boréave, M. Cazaunau, H.
641 Chen, V. Daële, J.F. Doussin, Y. Dupart, C. Gaimoz, C. George, B. Grosselin, H. Herrmann, S.
642 Ifang, R. Kurtenbach, M. Maille, A. Mellouki, K. Miet, F. Mothes, N. Moussiopoulos, L. Poulain,
643 R. Rabe, P. Zapf, J. Kleffmann, Photocatalytic de-pollution in the Leopold II tunnel in Brussels:
644 NO_x abatement results, Build Environ 84 (2015) 125-133. 10.1016/j.buildenv.2014.10.032

645 [52] M. Gallus, R. Ciuraru, F. Mothes, V. Akylas, F. Barmpas, A. Beeldens, F. Bernard, E.
646 Boonen, A. Boreave, M. Cazaunau, N. Charbonnel, H. Chen, V. Daele, Y. Dupart, C. Gaimoz, B.

Grosselin, H. Herrmann, S. Ifang, R. Kurtenbach, M. Maille, I. Marjanovic, V. Michoud, A. Mellouki, K. Miet, N. Moussiopoulos, L. Poulain, P. Zapf, C. George, J.F. Doussin, J. Kleffmann, Photocatalytic abatement results from a model street canyon, Environmental science and pollution research international 22 (2015) 18185-18196. 10.1007/s11356-015-4926-4

[53] M.V. Diamanti, R. Paolini, M. Rossini, A.B. Aslan, M. Zinzi, T. Poli, M.P. Pedeferri, Long term self-cleaning and photocatalytic performance of anatase added mortars exposed to the urban environment, Construction and Building Materials 96 (2015) 270-278. 10.1016/j.conbuildmat.2015.08.028

[54] M. Lettieri, D. Colangiuli, M. Masieri, A. Calia, Field performances of nanosized TiO_2 coated limestone for a self-cleaning building surface in an urban environment, Build Environ 147 (2019) 506-516. 10.1016/j.buildenv.2018.10.037

[55] M.M. Hassan, H. Dylla, L.N. Mohammad, T. Rupnow, Evaluation of the durability of titanium dioxide photocatalyst coating for concrete pavement, Construction and Building Materials 24 (2010) 1456-1461. 10.1016/j.conbuildmat.2010.01.009

[56] R. Zouzelka, J. Rathousky, Photocatalytic abatement of NO_x pollutants in the air using commercial functional coating with porous morphology, Applied Catalysis B: Environmental 217 (2017) 466-476. 10.1016/j.apcatb.2017.06.009

[57] A. Maury-Ramirez, K. Demeestere, N. De Belie, Photocatalytic activity of titanium dioxide nanoparticle coatings applied on autoclaved aerated concrete: effect of weathering on coating physical characteristics and gaseous toluene removal, J Hazard Mater 211-212 (2012) 218-225. 10.1016/j.jhazmat.2011.12.037

[58] H. Liu, B. Li, Z. Chen, T. Zhou, Q. Zhang, Solar radiation properties of common membrane roofs used in building structures, Materials & Design 105 (2016) 268-277. 10.1016/j.matdes.2016.05.068

[59] G. Zrim, M. Mihelčič, L.S. Perše, B. Orel, B. Simončič, R. Kunič, Light distribution in air-supported pneumatic structures: Comparison of experimental and computer calculated daylight factors, Build Environ 119 (2017) 110-127. 10.1016/j.buildenv.2017.04.005

[60] T. Shen, S. Li, Z. Wang, L. Wang, Rare bi-wetting TiO_2-F/SiO_2/F-PEG fabric coating for self-cleaning and oil/water separation, RSC Advances 6 (2016) 115196-115203. 10.1039/c6ra24474b

[61] R.A. Damodar, S.-J. You, H.-H. Chou, Study the self cleaning, antibacterial and photocatalytic properties of TiO_2 entrapped PVDF membranes, J. Haz. Mat. 172 (2009) 1321-1328. 10.1016/j.jhazmat.2009.07.139

[62] P. Kaner, X. Hu, S.W. Thomas, A. Asatekin, Self-cleaning membranes from comb-shaped copolymers with photoresponsive side groups, ACS Appl. Mater. Interfaces 9 (2017) 13619−13631. 10.1021/acsami.7b01585

[63] Y. Li, S. He, Z. Zhou, S. Zhou, S. Huang, A.G. Fane, C. Zheng, Y. Zhang, S. Zhao, Carboxylated nanodiamond-enhanced photocatalytic membranes with improved antifouling and self-cleaning properties, Ind. Eng. Chem. Res. 59 (2020) 3538-3549. 10.1021/acs.iecr.9b06389

[64] K.M. Sahlin, J.R. Greno, M.P. Cushman, R.C. Hobbs, J.M. McMartin, Composite article for use as self-cleaning material, US Patent Application US2014/0066289A1 (2014) https://patents.google.com/patent/US20140066289A1 (Accessed on: May 13, 2020)

[65] S. Chen, H.E. Gilbert, M. Truong, S. Houzé de l'Aulnoit, J. Zhang, G. Ban Weiss, R. Levinson, H. Destaillats, Solar Reflective "Cool" Walls: Benefits, Technologies and Implementation. Appendix J: Natural exposure of wall products (Task 4.2 Report), (2019). https://www.energy.ca.gov/2019publications/CEC-500-2019-040/

[66] NOAA, Global Historical Climatology Network (GHCN) (2018), National Oceanic and Atmospheric Administration., (Accessed on: May 13, 2020). https://www.ncdc.noaa.gov/data-

access/land-based-station-data/land-based-datasets/global-historical-climatology-network-ghcn

[67] CARB, Air Quality Data Statistics (2020), California Air Resources Board, (Accessed on: May 13, 2020). https://www.arb.ca.gov/adam

[68] SCAQMD, South Coast Air Quality Management District. AQ Detail – Historical Data. (2020), (Accessed on: May 13, 2020). https://xappprod.aqmd.gov/aqdetail/AirQuality/HistoricalData

[69] USEPA, Air data home. Pre-generated data files (2020), US Environmental Protection Agency, (Accessed on: May 13, 2020). https://aqs.epa.gov/aqsweb/airdata/download_files.html

[70] R. Levinson, H. Destaillats, S. Chen, P. Berdahl, H.E. Gilbert, Solar-Reflective "Cool" Walls: Benefits, Technologies, and Implementation. Appendix I: Metrics and methods to assess cool wall performance (Task 4.1 report), (2019). https://www.energy.ca.gov/2019publications/CEC-500-2019-040/

[71] Y. Qi, B. Xiang, J. Zhang, Effect of titanium dioxide (TiO_2) with different crystal forms and surface modifications on cooling property and surface wettability of cool roofing materials, Solar Energy Materials and Solar Cells 172 (2017) 34-43. 10.1016/j.solmat.2017.07.017

[72] A. Speziale, J.F. Gonzalez-Sanchez, B. Tasci, A. Pastor, L. Sanchez, C. Fernandez-Acevedo, T. Oroz-Mateo, C. Salazar, I. Navarro-Blasco, J.M. Fernandez, J.I. Alvarez, Development of multifunctional coatings for protecting stones and lime mortars of the architectural heritage, Int. J. Architectural Heritage. In press. Published online March 2020. 10.1080/15583058.2020.1728594

[73] M. Sleiman, T.W. Kirchstetter, P. Berdahl, H.E. Gilbert, S. Quelen, L. Marlot, C.V. Preble, S. Chen, A. Montalbano, O. Rosseler, H. Akbari, R. Levinson, H. Destaillats, Soiling of building envelope surfaces and its effect on solar reflectance - Part II: Development of an accelerated

720 aging method for roofing materials, Solar Energy Materials and Solar Cells 122 (2014) 271-281.
721 10.1016/j.solmat.2013.11.028

722 [74] J.Z. Bloh, A. Folli, D.E. Macphee, Photocatalytic NO_x abatement: why the selectivity
723 matters, RSC Adv. 4 (2014) 45726-45734. 10.1039/c4ra07916g

724 [75] S. Laufs, G. Burgeth, W. Duttlinger, R. Kurtenbach, M. Maban, C. Thomas, P. Wiesen, J.
725 Kleffmann, Conversion of nitrogen oxides on commercial photocatalytic dispersion paints,
726 Atmos. Environ. 44 (2010) 2341-2349. 10.1016/j.atmosenv.2010.03.038

727 [76] R.V. Mikhaylov, A.A. Lisachenko, B.N. Shelimov, V.B. Kazansky, G. Martra, S. Coluccia,
728 FTIR and TPD Study of the Room Temperature Interaction of a NO–Oxygen Mixture and of NO_2
729 with Titanium Dioxide, The Journal of Physical Chemistry C 117 (2013) 10345-10352.
730 10.1021/jp311593s

731 [77] O. Rosseler, M. Sleiman, V.N. Montesinos, A. Shavorskiy, V. Keller, N. Keller, M.I. Litter,
732 H. Bluhm, M. Salmeron, H. Destaillats, Chemistry of NOx on TiO_2 surfaces studied by ambient
733 pressure XPS: products, effect of UV irradiation, water, and coadsorbed K^+, J. Phys. Chem. Lett.
734 4 (2013) 536-541. 10.1021/jz302119g

735 [78] M.A. Kebede, M.E. Varner, N.K. Scharko, R.B. Gerber, J.D. Raff, Photooxidation of
736 ammonia on TiO2 as a source of NO and NO_2 under atmospheric conditions, Journal of the
737 American Chemical Society 135 (2013) 8606-8615. 10.1021/ja401846x

738 [79] L. Clarisse, M.W. Shephard, F. Dentener, D. Hurtmans, K. Cady-Pereira, F. Karagulian, M.
739 Van Damme, C. Clerbaux, P.-F. Coheur, Satellite monitoring of ammonia: A case study of the
740 San Joaquin Valley, Journal of Geophysical Research 115 (2010) D13302.
741 10.1029/2009jd013291

742 [80] A.R. Almeida, J.A. Moulijn, G. Mul, In Situ ATR-FTIR Study on the Selective Photo-
743 oxidation of Cyclohexane over Anatase TiO_2, The Journal of Physical Chemistry C 112 (2008)
744 1552-1561. 10.1021/jp077143t

745 [81] J. Araña, A.P. Alonso, J.M.D. Rodríguez, G. Colón, J.A. Navío, J.P. Peña, FTIR study of
746 photocatalytic degradation of 2-propanol in gas phase with different TiO_2 catalysts, Applied
747 Catalysis B: Environmental 89 (2009) 204-213. 10.1016/j.apcatb.2008.11.027

748 [82] Y. Luo, D.F. Ollis, Heterogeneous Photocatalytic Oxidation of Trichloroethylene and
749 Toluene Mixtures in Air: Kinetic Promotion and Inhibition, Time-Dependent Catalyst Activity,
750 Journal of Catalysis 163 (1996) 1-11. 10.1006/jcat.1996.0299

751

752